

Thermomechanical instability analysis of inhomogeneous deformation in amorphous alloys

Y.F. Gao^{a,b,*}, B. Yang^c, T.G. Nieh^{a,c}

^a Department of Materials Science and Engineering, University of Tennessee, Knoxville, TN 37996, USA

^b Computer Science and Mathematics Division, Oak Ridge National Laboratory, Oak Ridge, TN 37831, USA

^c Materials Science and Technology Division, Oak Ridge National Laboratory, Oak Ridge, TN 37831, USA

Received 12 June 2006; received in revised form 23 October 2006; accepted 14 November 2006

Available online 25 January 2007

Abstract

Recent experiments have shown that inhomogeneous deformation in amorphous alloys critically depends on the environmental temperature and the applied strain rate, and that the temperature field inside the shear-band can rise up to the glass transition temperature. A free-volume-based, thermo-viscoplastic constitutive law is developed in which the thermal transport equation includes contributions from the heating from plastic work and the heat conduction. For homogeneous deformation, the instantaneous temperature rise during the strain softening stage can lead to thermal softening and promote the initiation of shear bands. A linear stability analysis is carried out to examine the conditions for the unstable growth of temperature fluctuations. It is found out that the short-wavelength fluctuations, the amplitudes of which would decay at low strain rate and moderately high environmental temperature (but still much lower than the glass transition temperature), become unstable at high strain rate and low temperature, so that the resulting shear-band spacing will be shorter. A deformation mechanism map is constructed to delineate this transition of inhomogeneous deformation from coarse to fine shear-band arrangements. The theoretical results agree well with a nanoindentation experiment where there is varying applied strain rate and environmental temperature and with a microindentation experiment in which the evolution of the effective strain rate during loading influences the spatial distribution of the shear-band spacing observed using the bonded interface technique.

© 2006 Acta Materialia Inc. Published by Elsevier Ltd. All rights reserved.

Keywords: Metallic glasses; Shear bands; Thermomechanical constitutive model; Linear stability analysis; Shear-band spacing

1. Introduction

Strain localization into narrow shear bands leads to the inhomogeneous deformation mode in amorphous alloys (also called metallic glasses). Although details of atomistic mechanisms are still under debate, the shear-band formation is generally believed to be related to a stress-driven structural disordering process [1–4]. The resulting viscosity decrease will lead to strain softening behavior and subsequent strain localization. Under a uniaxial tension or com-

pression test, the shear band can propagate through a monolithic metallic glass specimen in a catastrophic manner, so that the macroscopic plastic deformation is hardly noticeable prior to the fracture failure. It is therefore anticipated that the increase in the number and density of shear bands could enhance the ductility and toughness of amorphous alloys. To this end, the constitutive response of the amorphous alloy under various geometric constraints, temperatures and strain rates should be examined with a direct connection to the individual processes that create and multiply shear bands [5–7].

The shear banding behavior was thought of as an isothermal process. However, recently a series of noteworthy experiments [8–11] illustrate the importance of the thermomechanical coupling behavior. Using the in situ thermogra-

* Corresponding author. Address: Department of Materials Science and Engineering, University of Tennessee, Knoxville, TN 37996, USA. Tel.: +1 865 974 2350; fax: +1 865 974 4115.

E-mail address: ygao7@utk.edu (Y.F. Gao).

phy technique, Yang and co-workers [8,9] found a temperature rise of 0.25 °C in a hot band of about 0.4 mm width. The shear-band width is typically found to be on the order of several tens of nanometers by electron microscopy measurement. Owing to local heating from the plastic work, it is estimated that the instantaneous temperature rise in a shear band can be as high as the glass transition temperature [9], as also shown by the observation of a melted coating layer adjacent to a shear band [10]. The radical difference from the thermography measurement is due to the slow data acquisition time (about 1.4×10^{-3} s) compared to the rapid heat conduction. Nanoindentation tests [11] show that, at high strain rate and low temperature, the density of shear bands increases (i.e. fine shear-band spacing) and the load–displacement curves show smaller amplitudes of serrations (macroscopically shown as “homogeneous” deformation). From those experiments, it is clear that, in order to understand the effects of temperature and strain rate and to analyze the in situ measurements of the evolution of the shear-band arrangements (by thermography with limited time and spatial resolutions), we need to develop a thermomechanical model that can model both stress-driven and thermally induced strain localization phenomena.

This paper is organized as follows. In Section 2, we first introduce a thermo-viscoplastic constitutive law that is based on the free volume model [3,4]. The plastic flow equation, the free-volume evolution equation and the thermal transport equation are functions of the stress, free volume and temperatures. If the deformation mode is homogeneous flow, those constitutive equations and the force–balance equation can be integrated with respect to time to examine the effects of temperature and strain rate. The local heating from the plastic energy dissipation will increase the temperature which further promotes the viscosity drop and shear-band initiation. For the inhomogeneous flow, the constitutive law, the force balance equation and the strain–displacement relation can be solved by the finite element method [7], which is beyond the scope of this paper. Instead, we perform a linear stability analysis from the homogeneous solution and derive the conditions for unstable growth of the temperature fluctuation, as shown in Section 3. With varying environmental temperature and applied strain rate, a deformation mechanism map will be constructed to delineate the transition from homogeneous to inhomogeneous deformation mode and the transition of the inhomogeneous deformation from coarse to fine shear-band spacing. To be specific, we have found that the shear-band spacing is small at high strain rate and low temperature. This theoretical result will be compared to two experiments: (1) a nanoindentation test showing the dependence of load–displacement serrations on temperature and strain rate [11] and (2) a microindentation test by the bonded interface technique showing the shear-band spacing [12]. In the former, our model differs from that in Ref. [11]; in the latter, only qualitative comparison can be made because of the lack of information

on the contact size evolution. Conclusions will be given in Section 4.

2. The thermo-viscoplastic constitutive model

Shear-band formation in amorphous alloy is related to the evolution of the local atomic structural order, although details of atomistic mechanisms for shear-band initiation are still under investigation. From the continuum mechanics standpoint, however, it is accepted that the shear band is one type of strain localization phenomena caused by strain softening. One microscopic model that captures this relationship is the free volume model. The free volume is the excess volume that atoms can freely move in and is defined as the average atomic volume minus the average atomic volume in the ideally ordered structure of atoms. The microscopic mechanism for the plastic flow is a result of a number of individual atomic jumps [3]. In the absence of applied force, the rates of forward and backward jumps of an atom into the neighboring vacancy are the same and obey an Arrhenius-type dependence on the activation energy. When the energy landscape is biased, there will be more jumps in one direction than the other. Consequently, the irreversible (viscous) part of the strain rate can be represented by the flow equation:

$$\dot{\gamma}^p = 2v \exp\left(-\frac{\alpha v^*}{v_f}\right) \exp\left(-\frac{\Delta G^m}{k_B T}\right) \sinh\left(\frac{\tau \Omega}{2k_B T}\right), \quad (1)$$

where $\dot{\gamma}^p = \partial \gamma^p / \partial t$, v is the frequency of atomic vibration, α is a geometrical factor of order 1, v^* is the critical volume (hard-sphere volume of an atom), v_f is the average free volume per atom, ΔG^m is the activation energy, Ω is the atomic volume, τ is the shear stress, k_B is the Boltzmann constant and T is the absolute temperature. The amount of energy bias on the energy landscape is $\tau \Omega$ in Eq. (1).

The viscosity is defined as $\eta = \tau / \dot{\gamma}^p$:

$$\eta = \frac{\tau}{2 \sinh(\tau \Omega / 2k_B T)} v^{-1} \exp\left(\frac{\alpha v^*}{v_f}\right) \exp\left(\frac{\Delta G^m}{k_B T}\right) \quad (2)$$

For the atomic structural disordering process, we consider the stress-driven free volume creation and the annihilation process by diffusional atomic jumps [3]. Without the evolution of the state variable, Eq. (1) will be the same as the standard viscoplasticity model and no strain softening will be developed. An atom can be squeezed into a neighboring small vacancy and thus a free volume can be created. Meanwhile, the free volume can be annihilated by diffusional atomic jumps. Consequently, the net rate of free volume increase is:

$$\dot{v}_f = v^* v \exp\left(-\frac{\alpha v^*}{v_f}\right) \exp\left(-\frac{\Delta G^m}{k_B T}\right) \left\{ \frac{2\alpha k_B T}{v_f \mu^*} \left[\cosh\left(\frac{\tau \Omega}{2k_B T}\right) - 1 \right] - \frac{1}{n_D} \right\} \quad (3)$$

where n_D is the number of atomic jumps needed to annihilate a free volume equal to v^* and is usually taken to be 3–10. The effective elastic modulus is $\mu^* = \frac{2}{3} \mu \frac{1+\nu}{1-\nu}$ with the shear

modulus μ and Poisson's ratio ν . The dependence of Eq. (3) on stress and temperature is shown below. If the temperature is a constant, the applied shear stress can overcome the annihilation term ($1/n_D$ in the braces), so that the free volume increases and the local viscosity in Eq. (2) decreases. As will be shown shortly, plastic deformation will lead to local heating and temperature increase. From elementary calculus, $\lim_{x \rightarrow 0} (\cosh x - 1)/x = 0$. Therefore, with an increase of temperature, the first term in the braces of Eq. (3) will eventually be less than the second one. In other words, with an increase of temperature, the process of free-volume annihilation by diffusional atomic jumps will overtake that of stress-driven free-volume creation, so that the weakening process (i.e. decrease in viscosity) will not occur. This transition occurs near the glass transition temperature.

Considering the experiments in Refs. [8–10], we can write down the thermal transport equation:

$$\rho C_P \dot{T} = k \frac{\partial^2 T}{\partial x^2} + \alpha_{TQ} \tau \dot{\gamma}^p \quad (4)$$

where ρ is the material density, C_P is the specific heat, k is the thermal conductivity and α_{TQ} is the fraction of the plastic work converted to heat (i.e. the Taylor–Quinney coefficient). The phenomenological parameter α_{TQ} is taken to be 0.9 in this paper. For this simple shear problem, the x coordinate is perpendicular to the shear direction (y coordinate), so that the shear stress τ is actually the stress component τ_{xy} .

Eqs. (1), (3) and (4) prescribe the constitutive law, which can be solved together with the force–balance equation:

$$\dot{\tau}/\mu + \dot{\gamma}^p = \dot{\gamma} \quad (5)$$

where $\dot{\gamma}$ is the applied strain rate and $\dot{\tau}/\mu$ gives the elastic strain rate. The decomposition of the total strain rate into elastic and plastic parts is equivalent to a spring and a dashpot in serial. The strain rate of interest is low enough so that the inertia force is ignored. For homogeneous deformation, the heat conduction term vanishes in Eq. (4), so that we can simply integrate those equations with respect to time. We use the backward Euler integration scheme, in which the unknown quantities are evaluated at the end of the time increment, i.e. at time $t_{n+1} = t_n + \Delta t$, where Δt is the time increment and n is the step number. The set of nonlinear ordinary differential equations will become a set of algebraic equations and the increments of stress, free volume and temperature can be computed using the Newton–Raphson method. The generalization of this integration scheme to multiaxial stress states can be found in Ref. [7].

To facilitate the understanding of numerical results, we normalize the temperature by the reference room temperature $T_0 = 300$ K, stress and shear modulus by $\tau_0 = 2k_B T_0 / \Omega$, free volume by av^* and time by $t_0 = v^{-1} \exp(\Delta G^m / k_B T_0)$. Consequently, we will naturally get three dimensionless parameters $\beta = v^* / \Omega$, $\Delta G^m / k_B T_0$ and $\alpha_{TQ} \tau_0 / \rho C_P T_0$ and a length scale $L = \sqrt{kt_0 / \rho C_P}$ in the normalized governing equations. The normalization of temperature by T_0 is just

a choice of convenience, since the glass transition temperatures for different metallic glasses are different. Following the work by Steif et al. [13], the geometric factor α is taken to be 0.15, the initial value of the normalized free volume v_f / av^* at $t = 0$ is around a few hundredths and we use $\beta = 1$, $\nu = 0.3$ and $n_D = 3$ in this paper. Changing these parameters does not qualitatively change our results. The parameter t_0 is the timescale on which the shear-band nucleation and propagation operate. There is some uncertainty about the activation energy, ΔG^m . Because of the exponential dependence, a slight change of ΔG^m will change the timescale t_0 by several orders of magnitude. The timescale is believed to range between 10^{-7} s and 10^{-5} s [3,4,9,13], so that the activation energy is a few tenths of an electronic volt. As a natural consequence of the timescale, $t_0 \dot{\gamma}$ will be the normalized strain rate and $L = \sqrt{kt_0 / \rho C_P}$ will be the heat conduction length from the thermal transport equation. Parameters k , ρ and C_P are estimated from experiments reported in Refs. [8,9].

The results for the homogeneous deformation mode are shown in Fig. 1, where solid lines are for the thermomechanical model and dashed lines are for the isothermal model (i.e. only Eqs. (1), (3) and (5) are considered, with $T = T_0$). For the isothermal case, there are three stages in the plots of stress τ / τ_0 and free volume v_f / av^* against the applied strain γ , shown in Fig. 1a and d, respectively. When the shear strain is small, the response is essentially elastic. From Eq. (3), the increase in shear stress drives the creation of the free volume and thus decreases the viscosity and weakens the material. Given a fixed applied strain rate, the strain softening behavior leads to the overshoot and the sharp turn on the stress–strain curve. After the peak stress, the decrease in shear stress slows down the increase in the free volume and eventually an equilibrium state is established in which there is no change of free volume. The dependence of the peak stress and the final free volume on the constitutive parameters and the applied strain rate has been thoroughly studied in Steif et al. [13]. Since temperature is fixed as a constant in the isothermal model, the instability index (as will be discussed later) is not applicable for this case.

The homogeneous deformation behavior originating from the thermomechanical model shows some similarities and differences when compared to that from the isothermal model. In the elastic region, the plastic work is negligible so that the temperature does not rise. Results from the two models are essentially the same during this stage. The subsequent stress increase drives the increase of free volume and leads to the strain-softening behavior. In the meantime, a large amount of plastic work is done and the temperature rises rapidly. The instantaneous temperature increase is plotted against the normalized applied strain rate in Fig. 2, showing how $\Delta T / T_0$ varies with respect to a five-decade strain-rate range. Beyond the overshoot, because of the accumulation of plastic work, the temperature keeps increasing. Next we will discuss the consequences of the temperature rise in these two stages.

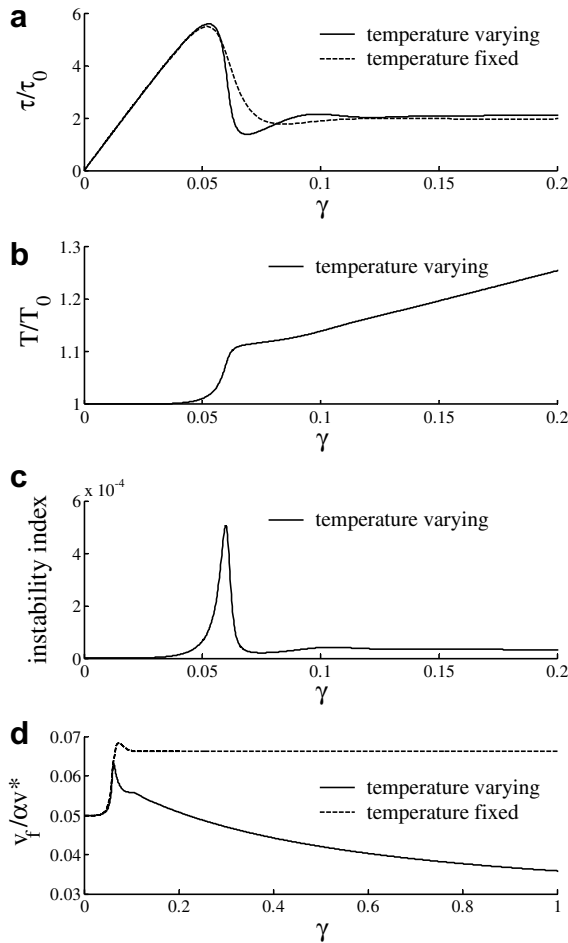


Fig. 1. The shear stress τ/τ_0 , the temperature T/T_0 , the instability index $\left(\frac{\partial \eta}{\partial T}\right) \tau \frac{\partial \gamma}{\partial t}$ and the free volume $v_f/\alpha v^*$ as a function of the applied shear strain γ , with $t_0 \dot{\gamma} = 2 \times 10^{-6}$, $\alpha = 0.15$, $\beta = 1$, $\mu/\tau_0 = 120$, $\nu = 0.3$, $n_D = 3$ and the initial free volume $v_i/\alpha v^* = 0.05$. The solid lines are obtained from the thermomechanical model and the dashed lines from the isothermal model (for which the instability index is not applicable). Note that the abscissa scale in (d) is different from other plots.

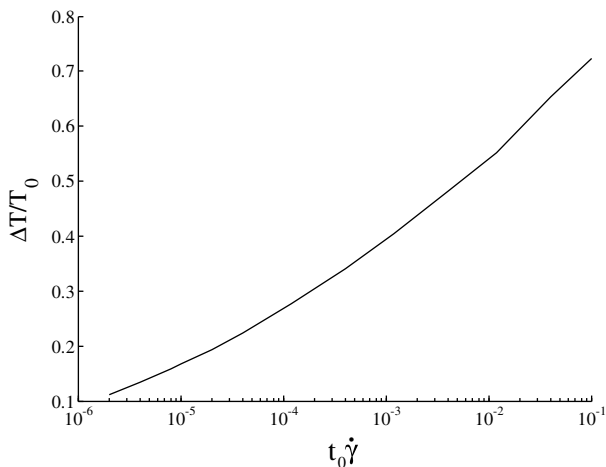


Fig. 2. The instantaneous temperature rise-up during the strain softening stage versus the applied strain rate.

From Eq. (2), the instantaneous temperature rise ΔT is equivalent to lowering the energy barrier, so that the viscosity will decrease facilitating shear-band nucleation and catastrophic failure of amorphous alloys. This agrees with the analysis in Ref. [9]. On the other hand, the temperature increase is also equivalent to lowering the work done by the applied force, so that the viscosity may increase. Whether or not thermal softening occurs is equivalent to determining if:

$$\frac{\partial \eta}{\partial T} = -\frac{\eta}{T} \left[\frac{\Delta G^m}{k_B T} - \frac{\tau \Omega}{2k_B T} \frac{\cosh(\tau \Omega / 2k_B T)}{\sinh(\tau \Omega / 2k_B T)} \right] \quad (6)$$

is < 0 . The two terms in the brackets correspond to thermally activated atomic jumps and the biased energy landscape due to the applied force, respectively. It is worthwhile examining the dependence of these two competing processes on the temperature and strain rate. Note that the function $x/\tanh(x)$ approaches 1 as $x \rightarrow 0^+$ and can be approximated by x as $x \gg 1$. With a given applied strain rate, high temperature (so that $\Delta G^m/k_B T \rightarrow 0$ and the second term in the brackets of Eq. (6) approaches 1) may lead to direct thermal hardening ($\partial \eta / \partial T > 0$). For this to happen, the temperature needs to be very high and close to the region of homogeneous deformation. A high applied strain rate will lead to a large τ_{\max}/τ_0 , since τ_{\max}/τ_0 is approximately proportional to $\log \left[\alpha \beta t_0 \dot{\gamma} \left(\frac{\mu}{\tau_0} \right)^2 \left(\frac{v_i}{\alpha v^*} \right)^3 e^{\alpha v^*/v_i} \right]$ where v_i is the initial value of v_f [13]. Therefore, a large $\dot{\gamma}$ may lead to $\partial \eta / \partial T > 0$. However, substituting realistic parameters from Table 1 shows that this will not occur unless the activation energy is so small as to be physically unrealistic. Consequently, for the case of inhomogeneous deformation, the instantaneous temperature rise will lead to a decrease in viscosity, i.e. $\partial \eta / \partial T < 0$.

After the sharp-turn region in Fig. 1a, the steady increase of the temperature will promote the annihilation of free volume, so that the free volume decreases and there is slight strain hardening (since $\partial \eta / \partial v_f < 0$) when γ is larger than about 0.15. It should be noted that the homogeneous flow, when the strain softening occurs, will be unstable, so that this indirect change of viscosity caused by free volume evolution in the last stage makes little contribution to the shear-band initiation. According to results in Fig. 1 and analyses in Ref. [9], it is the instantaneous temperature rise during the stage of strain softening, together with the stress-driven instantaneous free-volume rise, that govern the conditions for the homogeneous deformation to be unstable. The predicted temperature rise (from Fig. 2) ranges from 30 °C to 200 °C, corresponding to the prediction using the adiabatic condition in Ref. [9]. However, this is only a crude estimate; a rigorous calculation needs the solution of the set of partial differential equations given in Eqs. (1)–(5). To this end, we have to rely on numerical methods such as finite difference or finite element method, which is beyond the scope of this paper. In the next section, we illustrate an important consequence of the thermomechanical model, i.e. the conditions for the homogeneous solution to be unstable.

Table 1

Materials constants used in the thermo-viscoplastic constitutive law and the parameters used to normalize stress, time and length, i.e. $\tau_0 = 2k_B T_0 / \Omega$, $t_0 = v^{-1} \exp(\Delta G^m / k_B T_0)$ and $L = \sqrt{k \exp(\Delta G^m / k_B T_0) / \rho C_P v}$

T_0	ΔG^m	v	Ω	α_{TQ}	k	ρ	C_P	τ_0	t_0	L	$\alpha_{TQ} \tau_0 / \rho C_P T_0$
300 K	0.2–0.5 eV	10^{13} s^{-1}	$2 \times 10^{-29} \text{ m}^3$	0.9	20 W/(mK)	6810 kg/m ³	330 J/(kg K)	414 MPa	10^{-5} s	9.4 μm	0.553

3. Linear stability analysis and discussion

3.1. Linear stability analysis

The homogeneous solution can become unstable because of strain softening behavior. In this section, the shear-band initiation will be studied by a linear stability analysis and the effects of temperature and strain rate will be examined. Using the method in Refs. [14,15], the homogeneous solution can be perturbed to:

$$\gamma = \gamma_h(t) + \delta_\gamma(t) \exp(i\omega x) \quad (7a)$$

$$v_f = v_{fh}(t) + \delta_{v_f}(t) \exp(i\omega x) \quad (7b)$$

$$T = T_h(t) + \delta_T(t) \exp(i\omega x) \quad (7c)$$

where quantities with subscript “h” denote the homogeneous solutions (as shown in Fig. 1) and $i = \sqrt{-1}$. Substituting Eq. (7) into the governing equations and keeping the first order terms gives:

$$\frac{d\delta_\gamma}{dt} = \frac{\partial \dot{\gamma}^p}{\partial v_f} \delta_{v_f} + \frac{\partial \dot{\gamma}^p}{\partial T} \delta_T \quad (8a)$$

$$\frac{d\delta_{v_f}}{dt} = \frac{\partial \dot{v}_f}{\partial v_f} \delta_{v_f} + \frac{\partial \dot{v}_f}{\partial T} \delta_T \quad (8b)$$

$$\rho C_P \frac{d\delta_T}{dt} = -k\omega^2 \delta_T + \alpha_{TQ} \tau \left(\frac{\partial \dot{\gamma}^p}{\partial v_f} \delta_{v_f} + \frac{\partial \dot{\gamma}^p}{\partial T} \delta_T \right) \quad (8c)$$

The perturbation to the shear strain will amplify, i.e. $d\delta_\gamma/dt > 0$, as the perturbation to the free volume amplifies ($\delta_{v_f} > 0$), since $\partial \dot{\gamma}^p / \partial v_f$ is a positive definite. From Eqs. (1) and (6), $\frac{\partial \dot{\gamma}^p}{\partial T} = -\frac{\dot{\gamma}^p}{\eta} \frac{\partial \eta}{\partial T}$. As we have discussed in previous section, the instantaneous temperature rise will usually lead to a negative $\partial \eta / \partial T$ so that the perturbation to the shear strain will amplify as the perturbation to the temperature amplifies. Eqs. (8b) and (8c) are coupled together. If the environmental temperature is very high and the applied strain rate is very low, the term $\partial \dot{v}_f / \partial T < 0$ because of the rapid diffusional arrangements of atoms, so that strain localization is prevented and the deformation remains homogeneous. This is in accordance with the prediction by the free-volume model in Ref. [3] and the shear-transformation-zone model in Ref. [4]. The transition between two deformation modes is illustrated in Fig. 4, as will be shown shortly. The instantaneous temperature rise will lead to a dramatic drop in the viscosity and thus promote strain localization. The stress overshoot and the slope of the sharp turn in Fig. 1a determine the condition for the onset of unstable, inhomogeneous deformation. Consequently, an increase in temperature perturbation will favor the bifurcation from homogeneous to inhomogeneous

deformation modes. When the temperature is beyond T_g , our model does not formally apply and a new domain of viscous fluid flow occurs in this regime.

The perturbation to the temperature will amplify, i.e. $d\delta_T/dt > 0$, as the perturbation to the free volume amplifies ($\delta_{v_f} > 0$), since $\partial \dot{\gamma}^p / \partial v_f > 0$. If $\alpha_{TQ} \tau \frac{\partial \dot{\gamma}^p}{\partial T} > k\omega^2$, the temperature perturbation will grow. It is anticipated that we will find a critical wavelength above which the homogeneous deformation is unstable. The necessary condition for thermal instability is $\left(\frac{\alpha_{TQ} t_0}{\rho C_P} \right) \tau \frac{\partial \dot{\gamma}^p}{\partial T} > \omega^2 L^2$, so that a critical wavenumber is defined as:

$$\omega_{\text{crt}} L = \sqrt{\max \left[\left(\frac{\alpha_{TQ} t_0}{\rho C_P} \right) \tau \frac{\partial \dot{\gamma}^p}{\partial T} \right]} \quad (9)$$

below which (longer wavelength) thermal instability occurs. Physically, this means that the heat generated by the plastic work cannot be conducted sufficiently fast. To this end, $\left(\frac{\alpha_{TQ} t_0}{\rho C_P} \right) \tau \frac{\partial \dot{\gamma}^p}{\partial T}$ is called the instability index, as plotted in Fig. 1. Fig. 3 plots the critical wavenumber versus the normalized strain rate $t_0 \dot{\gamma}$. The critical wavenumber ω_{crt} increases as the strain rate increases, indicating that finer shear bands will appear at high strain rates. The relation between ω_{crt} and $\dot{\gamma}$ in Fig. 1 can be fitted by:

$$\omega_{\text{crt}} = \phi \sqrt{\frac{\rho C_P}{k}} v^{-\xi} \exp \left(\xi \frac{\Delta G^m}{k_B T} \right) \dot{\gamma}^{1/2+\xi} \quad (10)$$

where $\xi = 0.1066$ and $\phi = 74.4$. These two dimensionless parameters depend primarily on $\log \left[\alpha \beta t_0 \dot{\gamma} \left(\frac{\mu}{v_0} \right)^2 \left(\frac{v_i}{xv^*} \right)^3 e^{\alpha v^* / v_i} \right]$. From Eq. (10), given a fixed strain rate, the increase

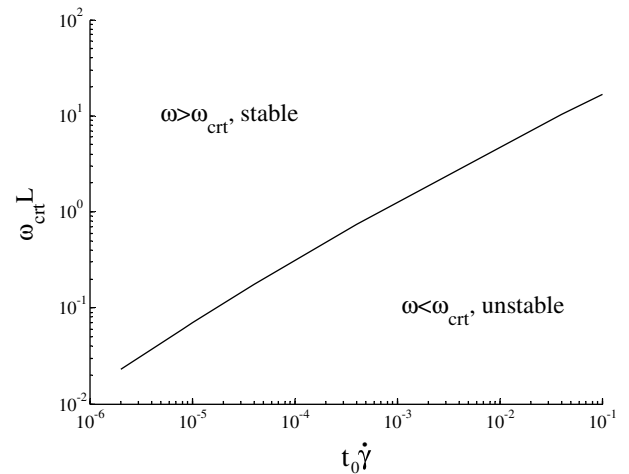


Fig. 3. Critical wavenumber in Eq. (9) versus the applied strain rate. As the strain rate increases, fluctuations of short wavelengths (which were stable at low strain rate) become unstable.

in the environment temperature will lower ω_{crit} . This suggests that fluctuations of short wavelength (which were unstable at low temperature) are now stable. In other words, the increase in temperature suppresses the initiation of fine shear bands.

3.2. Comparison to nanoindentation experiments and the construction of a deformation mechanism map

Our findings in Eqs. (9) and (10) can be used to explain the rate- and temperature-dependent deformation behavior observed from the nanoindentation experiments [11]. When the combination of the applied strain rate $\dot{\gamma}$ and the environmental temperature T is in the inhomogeneous region, as the increase of $\dot{\gamma}$ and the decrease of T , the load–displacement curves will show more frequent occurrences of serrations and the serration amplitudes decrease. The strain-softening-induced strain localization is one type of snap-back instability (similar to crack nucleation and dislocation emission), which will be revealed as discontinuities (or called serrations) on the load–displacement curves. To this end, the observations in Ref. [11] indicate the appearance of many closely spaced shear bands at high $\dot{\gamma}$ and low T . The deformation behavior is seemingly “homogeneous” in time. The transition from widely spaced to closely spaced shear bands is not actually modeled in Schuh et al. [11]. Their work is based on the shear transformation zone (STZ) model [4], in which the deformation occurs as a collective shear motion of a cluster of atoms. In Ref. [11], it is believed that the local strain field produced by the first STZ will affect the potential STZs nearby, so that a collection of multiple STZs can become a “shear-band nucleus” or “embryonic shear band”. When the applied strain rate exceeds the characteristic rate for shear-band nucleation (which is extensively modeled in Ref. [11]), there is not enough time for a shear band to nucleate, so that the deformation behavior will be homogeneous in both space and time. However, the experimental observation shows “homogeneous” deformation in time (as indicated by the smaller amplitudes of serrations) but still inhomogeneous in space (with multiple closely spaced shear bands). Consequently, the model in Schuh et al. [11] can only be applicable at extremely high strain rate and certainly cannot adequately explain their experiments, as the authors point out at the end of their paper.

The theoretical development in this paper aims to provide a mechanistic explanation of the dependence of shear-band spacing on the applied strain rate and temperature, a missing link in Ref. [11]. The instantaneous temperature rise during the onset of strain softening leads to a significant drop of viscosity and promotes the failure. Our linear stability analysis in Eq. (8) and Eq. (9) indicates that the homogeneous solution can be unstable because of the strain softening. According to Fig. 3, with an increase in the strain rate or a decrease in the temperature, temperature fluctuations of short wavelength (which were stable at low strain rate or at high temperature) become unstable, so

that the resulting shear-band spacing will be smaller. Physically this means that there is not enough time to annihilate the short-wavelength fluctuations if the loading rate is high (so that the rate of stress increase is high) or the temperature is low (so that the rate of atomic diffusion is low). Experiments in Refs. [8,9,11] suggest that the wavelengths of typical structural and temperature fluctuations are of tens of micrometers. Consequently, the strain rate increase under a given environmental temperature, or the temperature decrease under a given strain rate, will lead to the initiation of multiple and closely spaced shear bands, thus giving rise to temporally homogeneous behavior on the macroscopic stress–strain curves. The conventional free volume model or the STZ model does not have a length scale and thus cannot predict the shear-band spacing.

Eq. (10) can be used to construct a deformation mechanism map and to delineate the transition of inhomogeneous deformation from coarse to fine shear bands. As shown in Fig. 4, at very low strain rate and very high temperature, there is the transition from inhomogeneous to homogeneous deformation modes, as has been extensively studied in Refs. [3,4,11]. Strictly speaking, the homogeneous deformation mode means a stable homogeneous solution. The underlying mechanism for this transition is that at high T and low $\dot{\gamma}$, diffusive arrangements of atoms dominate and the free volume cannot be accumulated. The transition of inhomogeneous deformation from coarse to fine shear-band arrangements is not a sharp transition. The dashed line in Fig. 4a corresponds to the condition for the unstable growth of a given wavelength. We replace ω_{crit} by an initial perturbation of wavenumber ω_{init} in Eq. (10) and then fit it to the available experiments in Ref. [11]. Therefore, the ordinate in Fig. 4a is not normalized. Fig. 4b is given in normalized coordinates, on which each dashed line corresponds to the condition for a certain wavelength to become unstable.

The dashed line in Fig. 4a fits to the corresponding line in Fig. 5 of Ref. [11]. The latter actually denotes the experimental observations with the same degree of load–displacement serration under varying T and $\dot{\gamma}$. Our fitting procedure leads to the glass transition temperature $T_g = 490$ K and initial perturbation wavelength $\lambda_{\text{init}} = 0.8$ mm. The length λ_{init} is quite sensitive to the parameters chosen in the curve fitting because the ordinate $\dot{\gamma}$ is in logarithmic scale and Eq. (10) is an exponential function of $\Delta G^{\text{m}}/k_B T$. Choosing $\omega_{\text{init}} L = 0.36$ will move up the dashed line by one decade and the length λ_{init} is estimated to be 160 μm . The length scale L is the heat conduction length associated with $t_0 = 10^{-5}$ s. From Refs. [4,9], the characteristic time to activate individual shear transformation zone is 3.3×10^{-7} s and the associated length will be 1.7 μm . Repeating the calculations in Figs. 3 and 4, we can estimate the perturbation wavelength to be $\lambda_{\text{init}} \approx 10$ μm . If the unit event for plastic deformation is the shear transformation zone, the activation energy can be very low so that the resulting length scale may approach nanometer length scale. Finally, we should point out that the shear modulus is assumed to be a constant in the linear

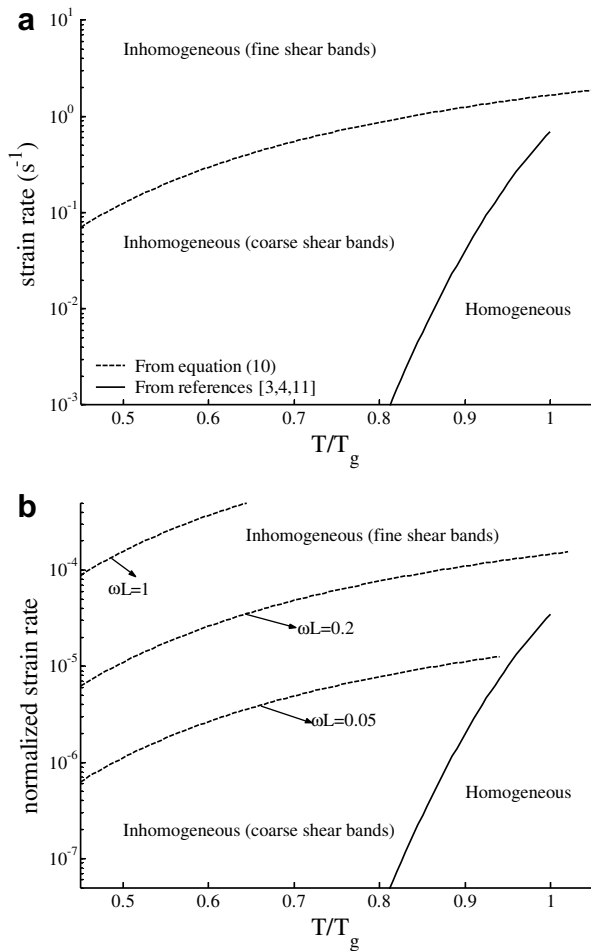


Fig. 4. Deformation mechanism map with respect to varying environmental temperature and applied strain rate. The transition from homogeneous to inhomogeneous deformation modes occurs at high temperature and low strain rate. The dashed line shows the condition for unstable growth of a given wavelength, illustrating the transition from coarse to fine shear-band arrangements. With very fine shear-band arrangements, the macroscopic stress–strain curve appears to be “homogeneous” in time. (a) The dashed line fits the experiments in Ref. [11]. (b) Unstable conditions for perturbations with different wavelengths with respect to the normalized strain rate ($\dot{\epsilon}_0 \dot{\gamma}$).

stability analysis. The construction of the boundary between homogeneous and inhomogeneous deformation has taken the temperature dependence of shear modulus into consideration, which is not anticipated to change our results on shear-band spacing qualitatively.

3.3. Comparison to shear-band spacing observation in a microindentation experiment

Our theoretical results can also be qualitatively confirmed by a microindentation experiment [12], in which the shear-band arrangements underneath the indenter can be observed using the bonded interface technique. First, Zr-based bulk metallic glass ($Zr_{52.5}Cu_{17.9}Ni_{14.6}Al_{10.0}Ti_{5.0}$) $3 \times 3 \text{ mm}^2$ square ingots were prepared by the arc melting and drop casting method. The ingot surfaces were polished to a mirror finish and then were bonded together with a

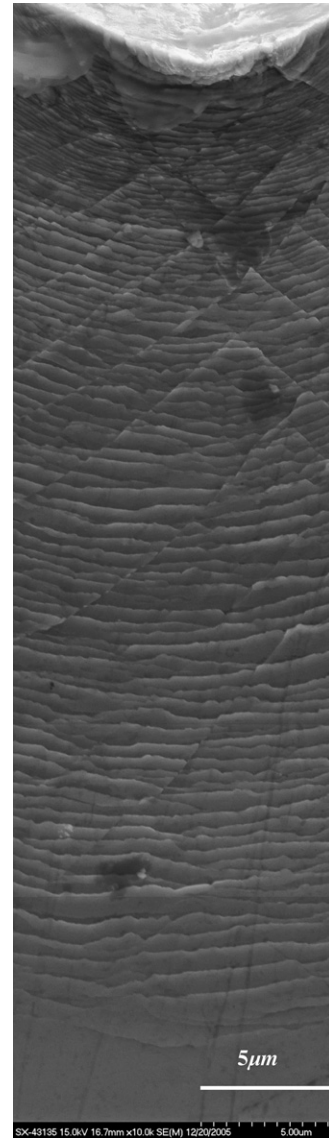


Fig. 5. Scanning electron microscopy image of the shear-band arrangement underneath a micro-contact. This cross-section observation is made available by the bonded interface technique.

rapid glue under a tight clamping force. The bonded ingots were mounted into epoxy. After the epoxy solidified, the top surface of the sample was polished to a mirror finish for the microindentation test. We used a Micromet[®] 2001 Tester and a pyramidal indenter. The test was under a Heaviside loading history (1 kg dead weight), so that the average contact pressure decreased and the contact size increased with time. After the test, the sample was cut out of the epoxy mounting and the rapid glue was dissolved into acetone. Using scanning electron microscopy (SEM), the shear-band arrangements on the cross-section can be observed, as shown in Fig. 5. Two types of shear bands were observed. The semi-circular shear bands are caused by the anti-plane shear because the interface glue can significantly relax the out-of-plane normal stress. The radial shear bands are believed to be due to in-plane shear. We are concerned with the former because the shear bands

do not cross each other, similar to what happens in our simple shear model. To understand these radial shear bands, we need to solve the boundary value problem in multi-axial stress states, e.g. by using the finite element method in Ref. [7]. The spacing of the semi-circular shear bands is plotted against the depth from the contact center in Fig. 6. The shear band spacing, which varies from about 0.1 μm to 1 μm over a range of 40 μm depth, is found to increase almost linearly beyond the small contact zone influenced by the tip bluntness. A similar trend has also been reported in Ref. [16]. It should be noted that fitting Fig. 4 to the experimental results in Ref. [11] gives rise to $\lambda_{\text{init}} = 10\text{--}100 \mu\text{m}$, which is considerably larger than that observed in Fig. 5.

In previous subsections, we have predicted that the shear-band spacing will decrease if the strain rate increases. This can be qualitatively shown from Fig. 5. Unfortunately, the strain-rate information and the contact size history are not available from this microindentation experiment [12]. For this self-similar indentation, the effective strain rate is given by $\dot{\epsilon}_{\text{eff}} = \dot{h}/h$ where h is the indentation depth. The relation between $\dot{\epsilon}_{\text{eff}}$ and the rate-dependent constitutive law is often very complex and is available only for a limited number of cases [17,18]. For example, consider a power-law creeping solid, $\sigma = \sigma_0(\dot{\epsilon}^p/\dot{\epsilon}_0)^{1/m}$, where σ_0 , $\dot{\epsilon}_0$ and m are constitutive parameters. The evolution of the mean pressure will be $p_m = F(m)\sigma_0(\dot{\epsilon}_{\text{eff}}/\dot{\epsilon}_0)^{1/m}$ where $F(m)$ is a function of the material parameter, m . This relation holds regardless of the loading condition (either fixed load rate or displacement rate), as long as the effective strain rate can be computed. In addition, if a dead weight is applied, the contact pressure varies with time t as $p_m \propto t^{-1/m}$ [18]. The total period of time for the contact to reach equilibrium and settle down is in a range of 5–30 s. Consequently, for the loading condition of a dead weight, the initial growth rate of the contact size and the resulting effective rate will be higher than that in the later stage. Thus the near-tip region will experience a higher effective strain rate than that away from the tip and

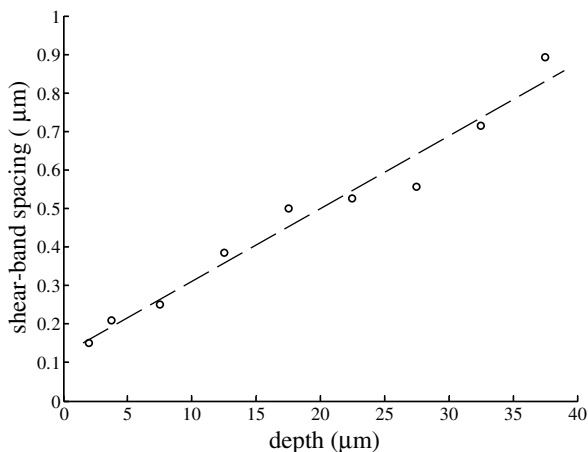


Fig. 6. The spacing of the semi-circular shear bands in Fig. 5 is roughly linear with the depth away from the contact center. The trend is shown by the dashed line.

will have more closely spaced shear bands as we have predicted in Fig. 4. This is confirmed by the observation in Fig. 6.

4. Conclusions

This paper develops a thermo-viscoplastic constitutive framework to understand the temperature evolution during homogeneous deformation and the effects of temperature and strain rate on the initiation of inhomogeneous deformation.

- At high temperature and low strain rates, the local stress-driven free-volume creation process can be easily overtaken by the annihilation process by diffusional atomic jumps, leading to homogeneous deformation. On the other hand, free volume accumulation, if it occurs, can weaken the material and lead to strain softening and inhomogeneous deformation. The transition between the homogeneous and inhomogeneous deformation modes has been thoroughly studied in Refs. [3–7].
- As in the experiments and theoretical estimate in Refs. [8,9], the strain softening behavior will lead to an instantaneous temperature rise which further promotes thermal softening and aids the initiation of inhomogeneous deformation. For inhomogeneous deformation, the increase of strain rate and the decrease of temperature can promote the initiation of multiple and closely spaced shear bands, as indicated by Fig. 3. Based on linear stability analysis, we have identified this transition from coarse to fine shear bands on a deformation mechanism map in Fig. 4.
- The deformation mechanism map qualitatively explains the dependence of shear-band spacing on the applied strain rate and the temperature. It agrees very well with the two experiments. In a nanoindentation experiment, the increase of applied strain rate and the decrease of the environmental temperature will lead to the appearance of closely spaced shear bands. The shear-band spacing was not modeled in Ref. [11]; our results in Figs. 3 and 4 offer this information. In a microindentation experiment, although the quantitative information of strain-rate history is not available, qualitatively the near tip region is anticipated to experience a higher effective strain rate than that away from the tip, which explains the observation in Figs. 5 and 6 (shear-band spacing observed by the bonded interface technique).

Acknowledgements

This work was supported in part by the University of Tennessee and the Tennessee Advanced Materials Laboratory. This work was also sponsored by the Division of Materials Sciences and Engineering, Office of Basic Energy Sciences, US Department of Energy, under contract DE-AC05-00OR22725 with UT-Battelle, LLC for our work performed at Oak Ridge National Laboratory and under

contract DE-FG02-06ER46338 for our work performed at the University of Tennessee. The authors are grateful to the anonymous reviewer for help in improving the quality and clarity of this paper.

References

- [1] Johnson WL. *MRS Bull* 1999;24:42.
- [2] Inoue A. *Acta Mater* 2000;48:279.
- [3] Spaepen F. *Acta Metall* 1977;25:407.
- [4] Argon AS. *Acta Metall* 1979;27:47.
- [5] Anand L, Su C. *J Mech Phys Solids* 2005;53:1362.
- [6] Yang Q, Mota A, Ortiz M. *Comput Mech* 2006;37:194.
- [7] Gao YF. *Modelling Simul Mater Sci Eng* 2006;14:1329.
- [8] Yang B, Liaw PK, Wang GY, Morrison ML, Liu CT, Buchanan RA, et al. *Intermetallics* 2004;12:1265.
- [9] Yang B, Liu CT, Nieh TG, Morrison ML, Liaw PK, Buchanan RA. *J Mater Res* 2006;21:915.
- [10] Lewandowski JJ, Greer AL. *Nature Mater* 2006;5:15.
- [11] Schuh CA, Lund AC, Nieh TG. *Acta Mater* 2004;52:5879.
- [12] Yang B, Nieh TG. Unpublished experiments; 2006.
- [13] Steif PS, Spaepen F, Hutchinson JW. *Acta Metall* 1982;30:447.
- [14] Shawki TG, Clifton RJ. *Mech Mater* 1989;8:13.
- [15] Huang R, Suo Z, Prevost JH, Nix WD. *J Mech Phys Solids* 2002;50:1011.
- [16] Ramamurty U, Jana S, Kawamura Y, Chattopadhyay K. *Acta Mater* 2005;53:705.
- [17] Mayo MJ, Nix WD. *Acta Metall* 1988;36:2183.
- [18] Bower AF, Fleck NA, Needleman A, Ogbonna N. *Proc Roy Soc London A* 1993;441:97.